Fermilab

TM-721-A
2125.000

A SEGMENTED HADRON CALORIMETER FOR USE AS A HIGH TRANSVERSE MOMENTUM "JET" TRIGGER

P. M. Mantsch, R. Krull, P. J. Limon, P. M. Mocket
J. R. Orr, S. Pruss, K. Young

May 1, 1978
Revised: September 6, 1979

I. INTRODUCTION

The observation of an unexpectedly high cross section for high transverse momentum particles in hadron hadron collisions has led to an extensive program to probe the fundamental structure of hadrons. This study has revealed clusters or "jets" of correlated high P_t particles raising the speculation that hard collisions of structureless fundamental constituents of hadrons are being observed. Assuming that jets are in fact fragments of scattered constituents (quarks or partons) these particles taken together may contain momentum and angle information on the constituent interaction itself. Until recently, experiments studying jet phenomena have triggered on a single high P_t particle. A total energy calorimeter, segmented to include an angle measurement is a device for triggering directly on high transverse momentum jets.

The calorimeter described below was built as part of an experiment designed to investigate the physics of hadron jets. The apparatus shown in the sketch in Fig. 1 consisted of two arms. On the right was a small solid angle ($\sim$1 str) magnetic spectrometer with particle identification and on the left was a segmented hadron calorimeter. The beam particles incident on the hydrogen target were tagged by Čerenkov counters in the beam. Figure 2 shows the laboratory angular region subtended by the spectrometer and calorimeter as seen from the target.

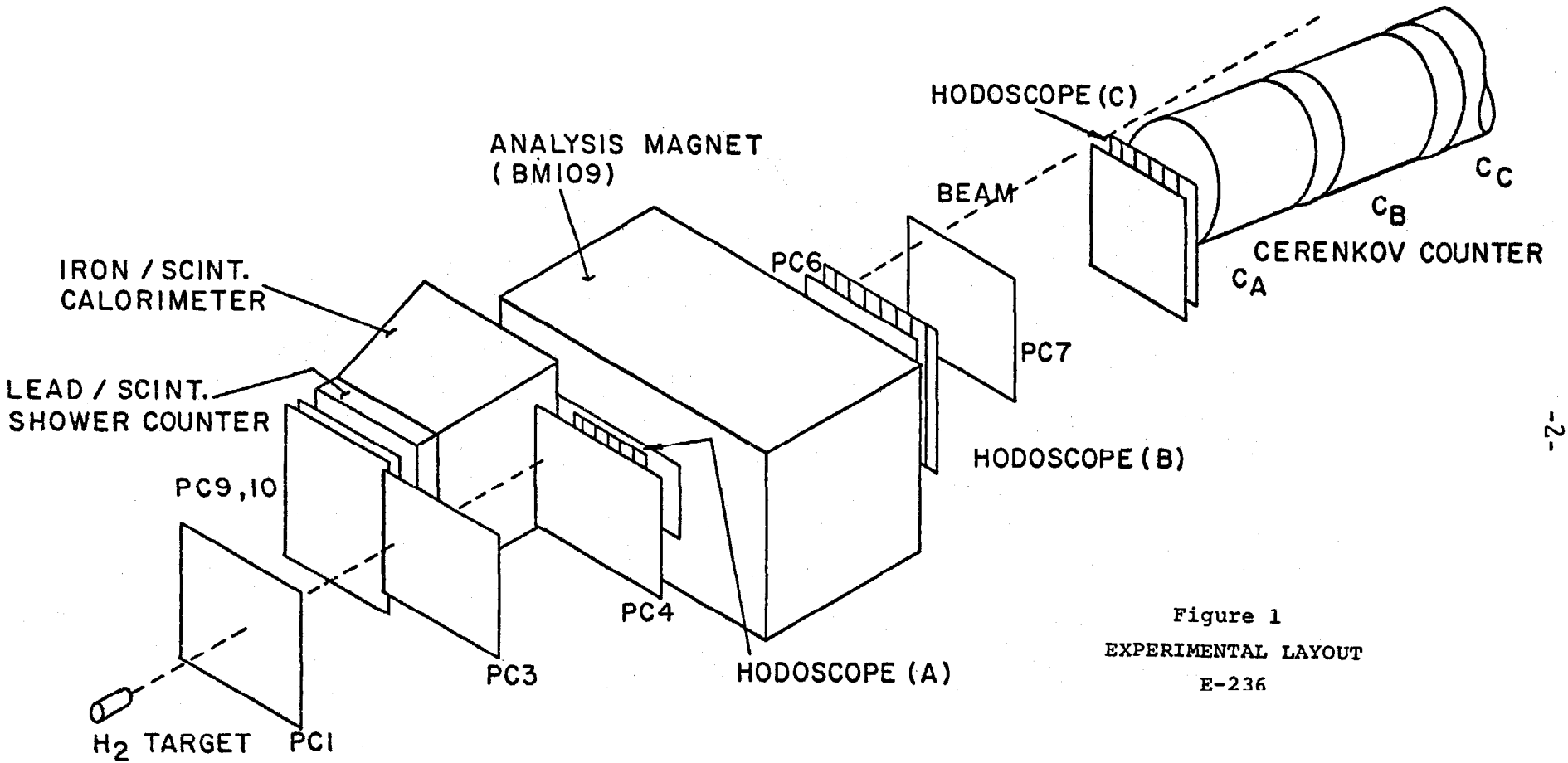

Figure 1
EXPERIMENTAL LAYOUT
E-236

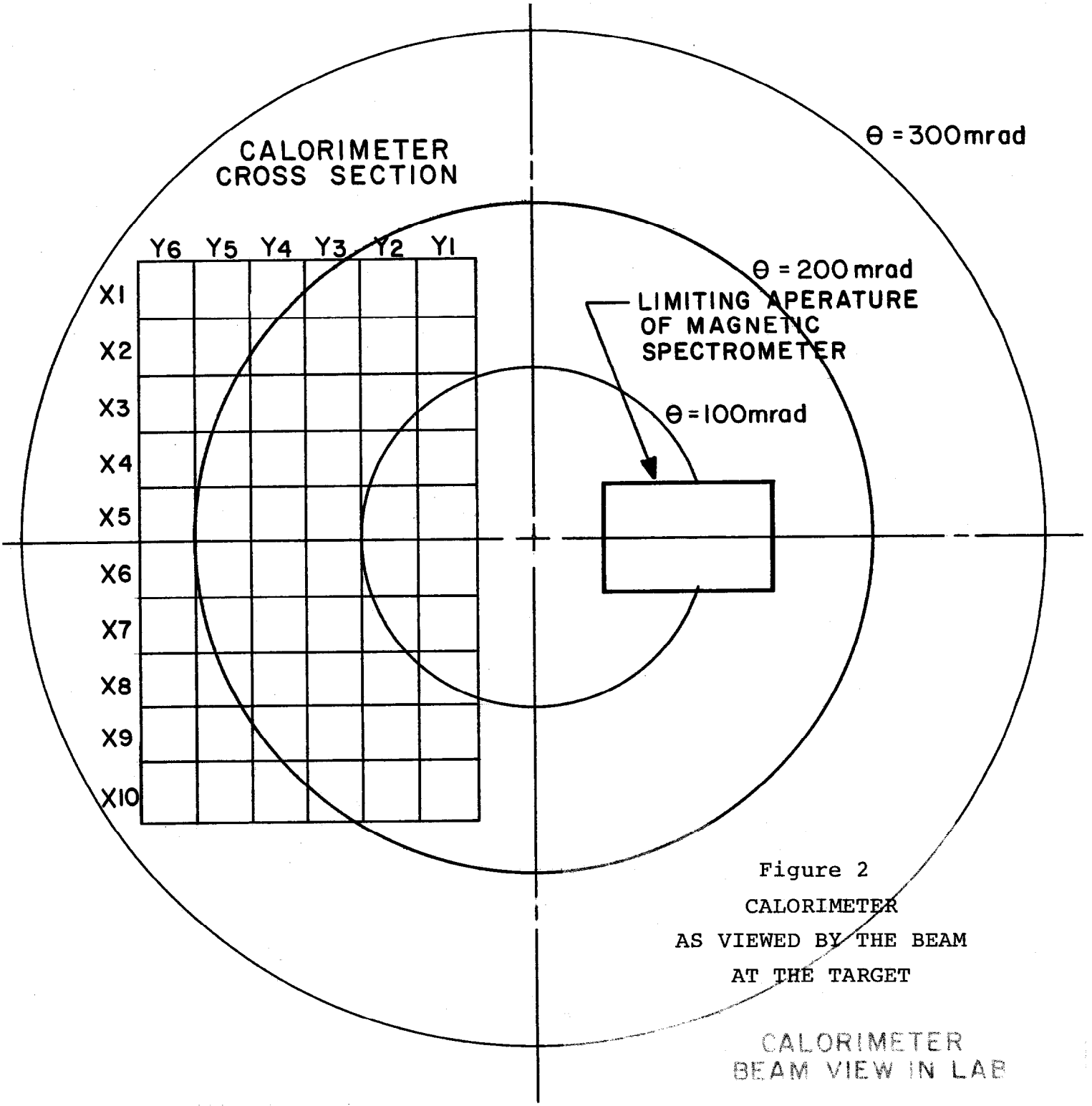

Figure 2

CALORIMETER

AS VIEWED BY THE BEAM

AT THE TARGET

The objectives of the experiment were the following:

The high P_t variation of the single particle cross section with particle species (both incoming and outgoing) was measured with the spectrometer to P_t of 4 GeV/c. The calorimeter measured the jet P_t cross section. The combination of the magnetic spectrometer and the calorimeter measured the P_t asimuthal and zenith angle correlation of events with high P_t particles and jets.

II. DETAILS OF CALORIMETER CONSTRUCTION

The calorimeter was divided into electromagnetic and hadronic sensitive parts. The electromagnetic detector consisted of alternate layers of lead and scintillator while the hadronic detector was steel and scintillator. Both the lead and steel detectors were divided into ten horizontal and six vertical segments. Light summed along the longitudinal shower development was collected from the strips comprising each segment. Figure 3 shows the essential features of the calorimeter while the specifications are listed in Table I.

Typical counter modules are shown in Fig. 4. Since the signal outputs of the photomultiplier tubes were to be used directly for a trigger, it was important that the response of each strip be independent of the position along the strip. The position response was studied in some detail and tests were performed first with a source and later with a well collimated beam. A number of techniques were used to achieve response uniformity along the counters:[1]

1) A reflector at the far end of each scintillator strip flattened the response at the far end.

2) A one-inch wide angle mask was painted on the light pipe

TABLE I

E-236 CALORIMETER

Area:	Front: 20.4" wide x 43.88" high	
	Back: 29.1" wide x 43.88" high	
Position:	102 inches from the target	
Angular Acceptance in the Laboratory:	Horizontal: $\approx$ 58 mr to 253 mr Vertical: $\approx \pm$ 212 mr ($\sim$ 3 str in CM)	
	Electromagnetic Detector	Hadronic Detector
Interaction Material/Detector	Lead/Scintillator (Pilot Y)	Iron/Scintillator (Pilot Y)
Segmentation	10 horizontal modules 4" wide x 20.4" long x 4 elements deep	10 horizontal modules 4" wide x 29.1" long x 16 elements deep
	6 vertical modules 3.4" wide x 40.25" long x 4 elements deep	6 vertical modules 3.4" wide x 40.25" long (front); 4.8" wide x 40.25" long (back) x 16 elements deep
Sample interval	1/4" Pb, 1/4 scintillator	1" Fe, 1/4" scintillator
Total samples	8	32
Radiation/Collision Length	10.2 rad. lengths 0.27 nuclear absorption lengths	5.04 nuclear absorption lengths

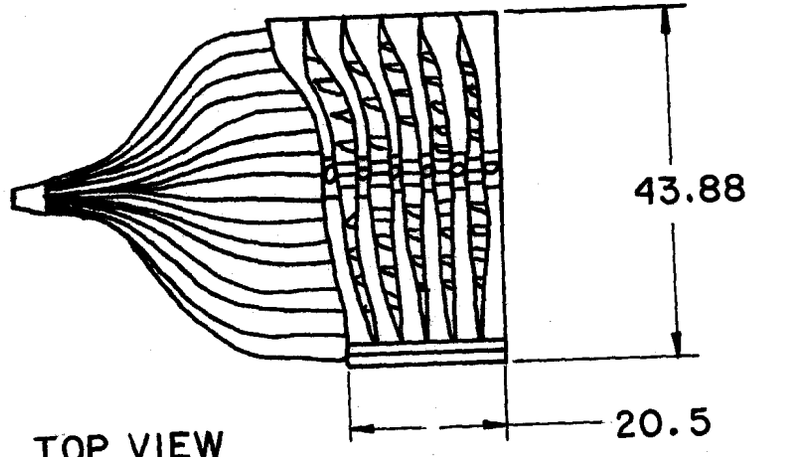

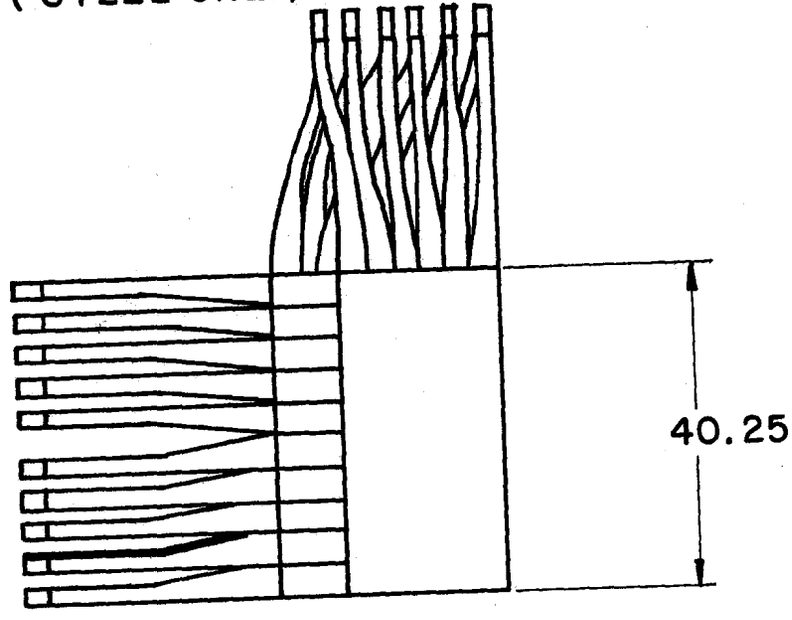

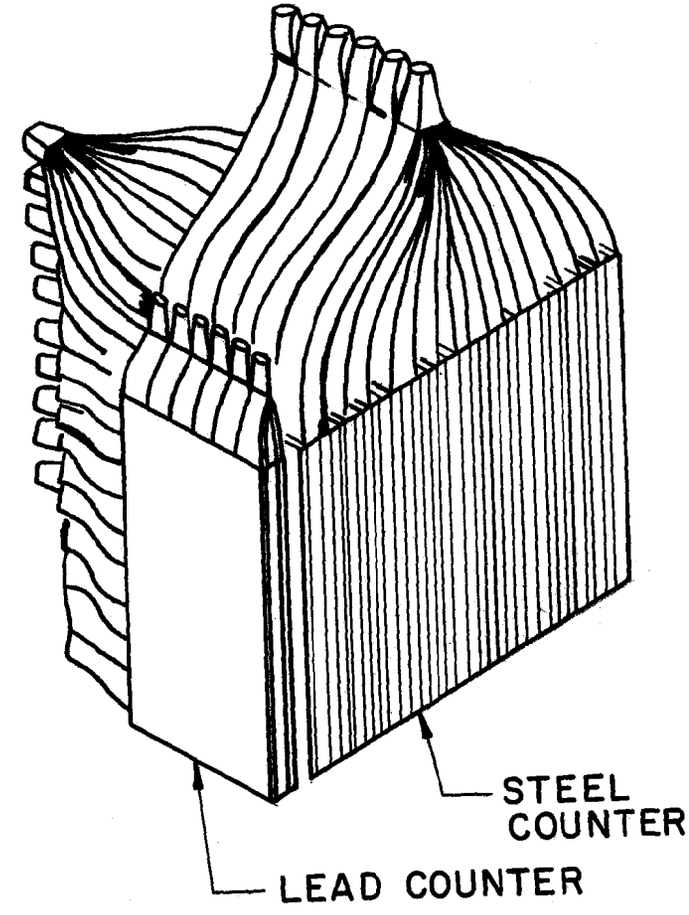

Figure 3

E-236 HADRON CALORIMETER

Figure 4

DETAILS OF CALORIMETER SCINTILLATOR MODULES

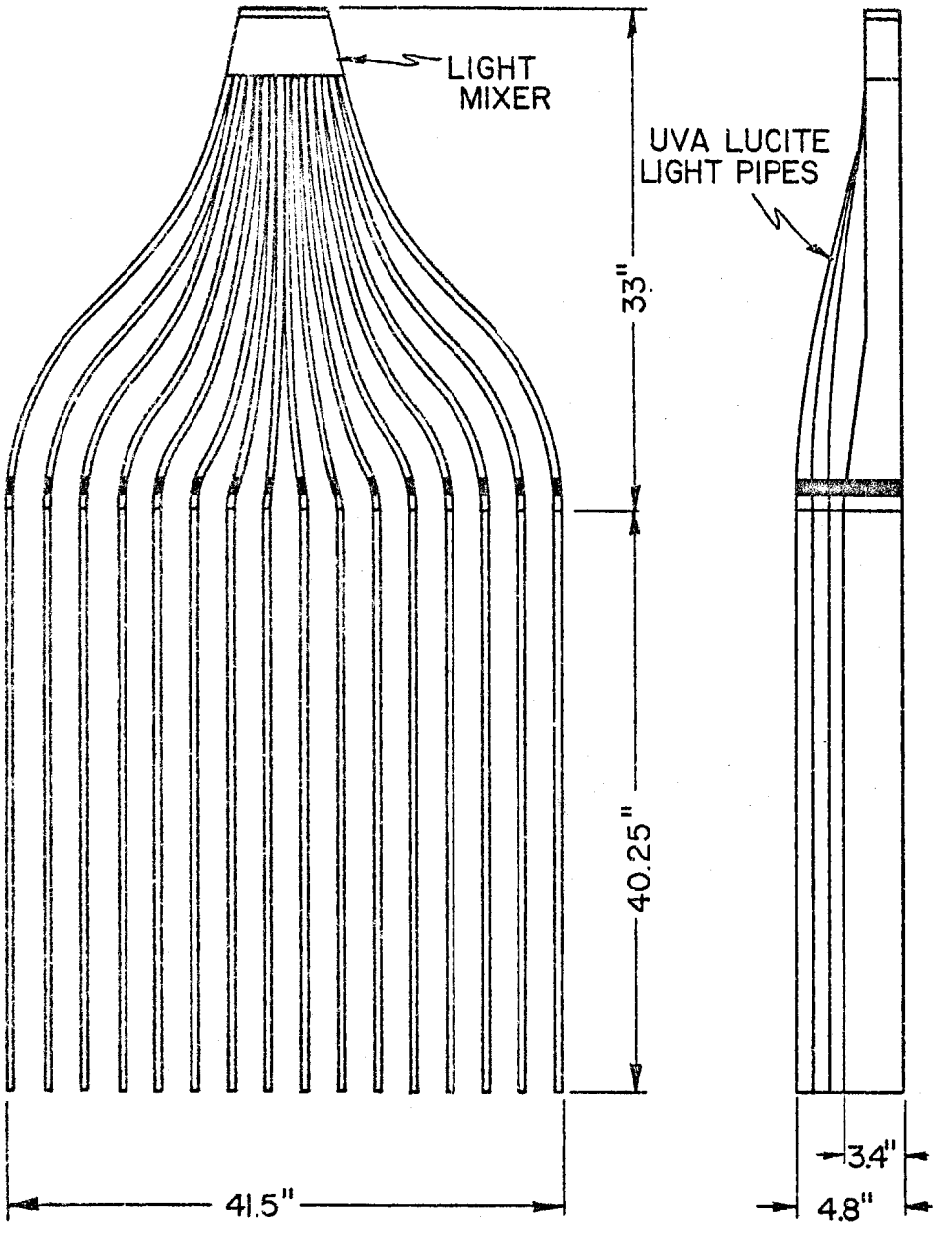

TYPICAL SCINTILLATOR MODULE USED IN THE STEEL COUNTER

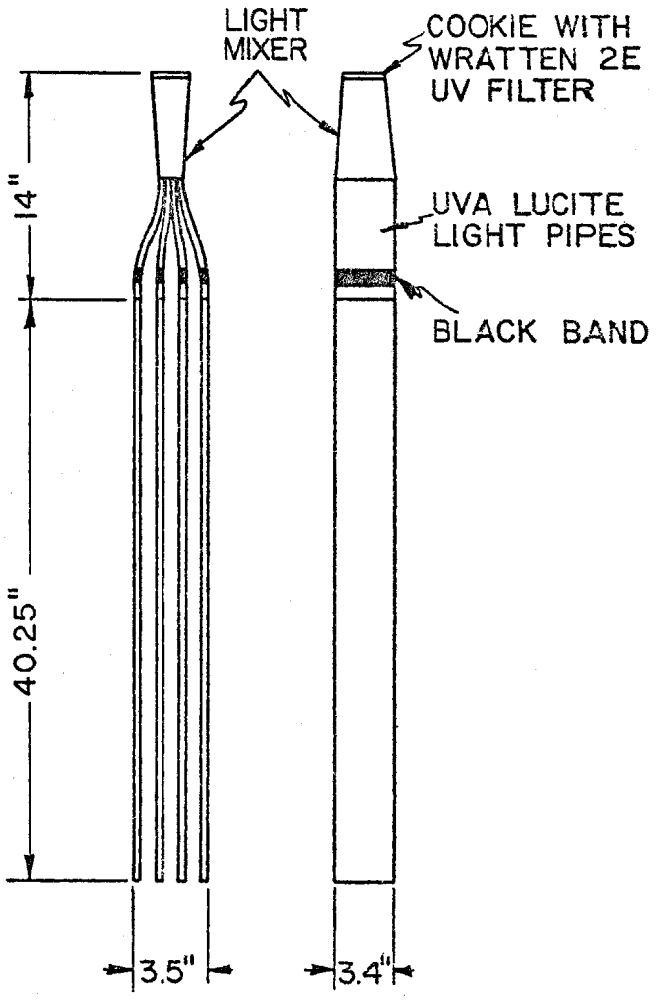

TYPICAL SCINTILLATOR MODULE USED IN THE LEAD COUNTER

1/4-inch from the scintillator/light pipe connection to absorb large angle rays.

3) Short-wave length light preferentially absorbed in the scintillator was removed with a Wratten 2E filter on the face of the photo tube.

These devices taken together reduced the light output by a factor of about 5. Figure 5 shows the response of one strip of scintillator under various conditions using a Ru^{106} beta source.

Once the modules for the lead counter were assembled, they were tested in a beam of minimum ionizing particles (without lead). Figure 6 shows the response of both a 20" long horizontal module and one of the vertical 40" long counters. Up to about four-inches from the phototube end of the counter, the response is flat within $\pm$ 3%. In the four inches nearest the tube, the response increases by about 10%.

The lead plates were assembled with aluminum spacers and bolts. The steel plates for the calorimeter were welded to a steel base with 3/8-inch spacing. The modules were then inserted into the gaps between the lead or iron plates and the whole assembly wrapped again to eliminate light leaks.

A number of photomultiplier tubes were studied for use on the calorimeter to find one with the least objectional drift characteristics. The RCA 6342A proved to be the best choice. The method for testing the tubes and gain drift results for the 6342A are described elsewhere.[2]

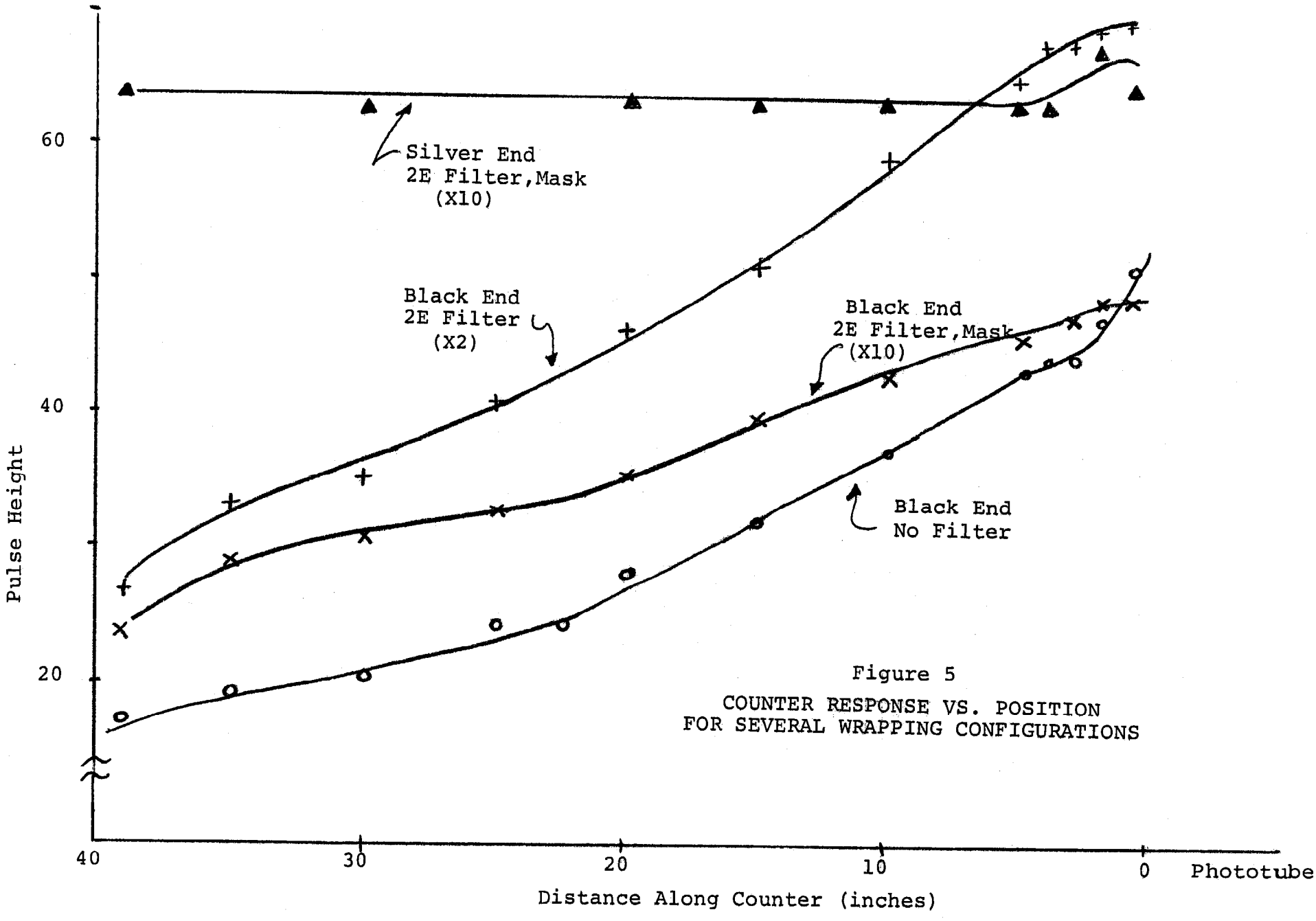

Figure 5

COUNTER RESPONSE VS. POSITION
FOR SEVERAL WRAPPING CONFIGURATIONS

Figure 6

SHOWER COUNTER UNIFORMITY TESTS

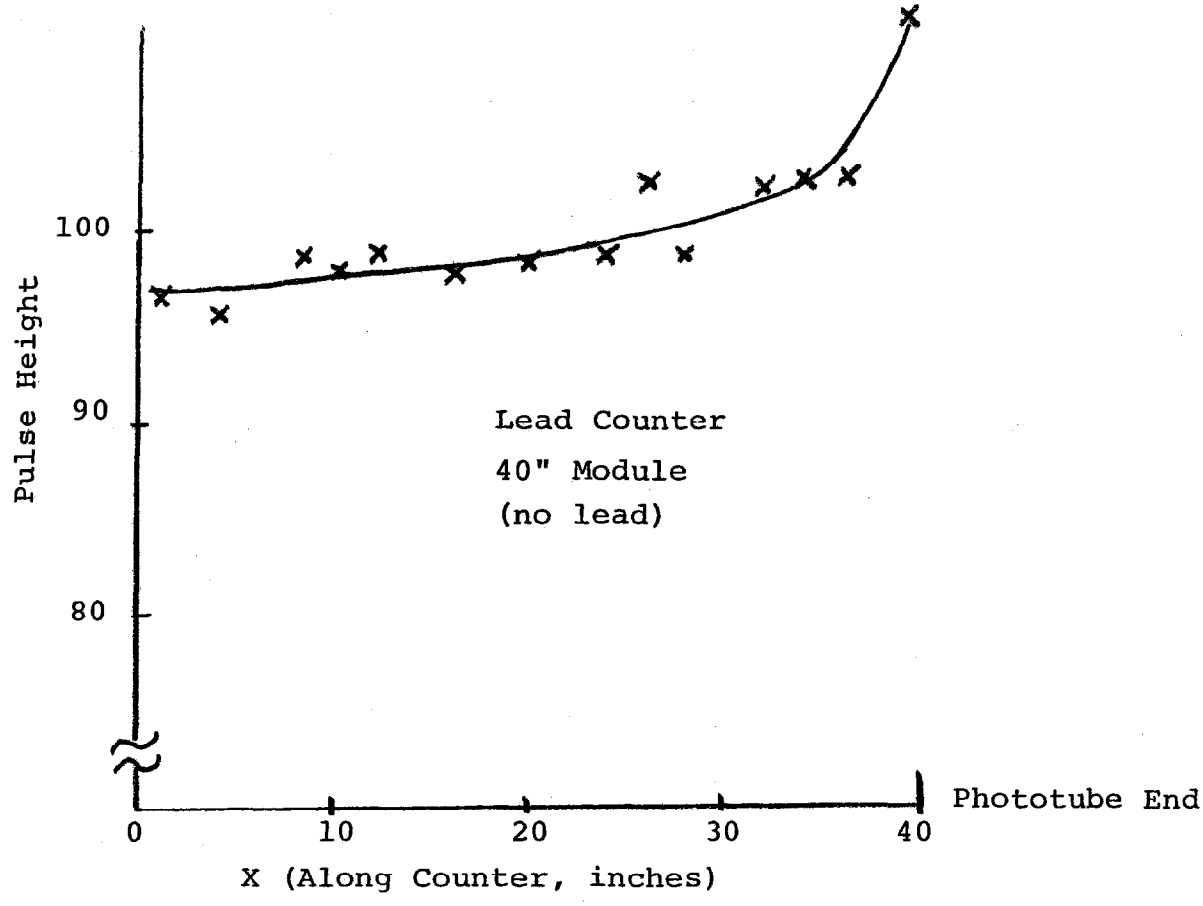

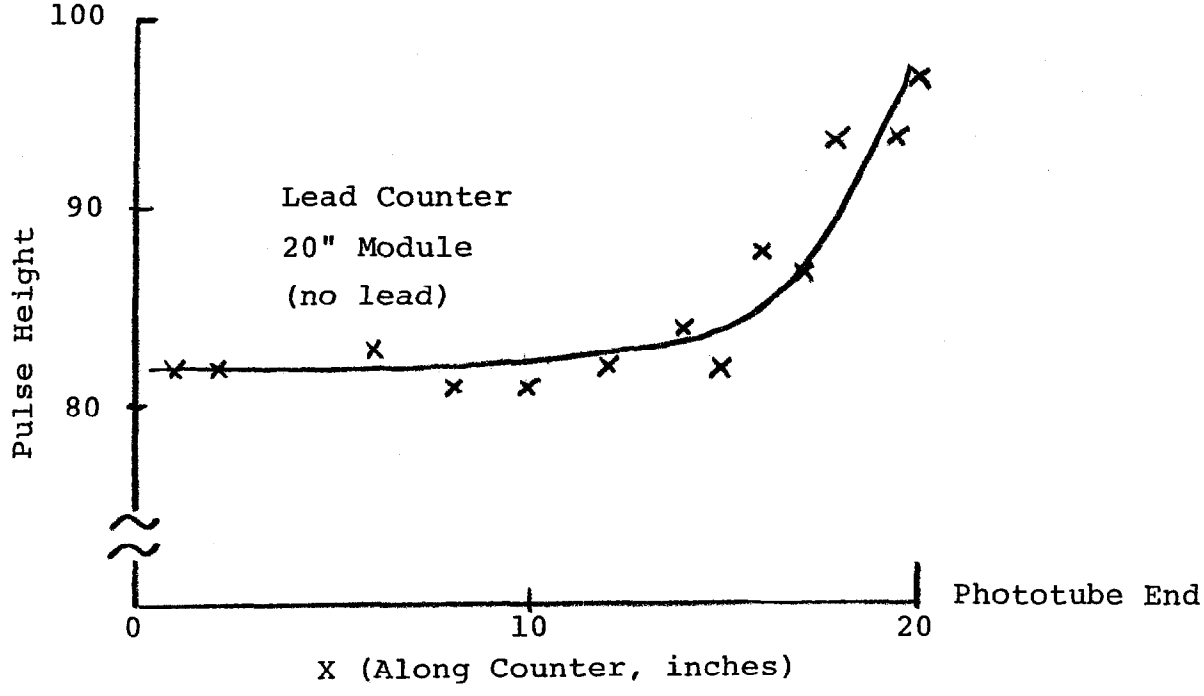

III. PHOTOTUBE GAIN MONITOR SYSTEM

A light flasher system was built into the detector to maintain the calibration of the counters for accurate P_t determination both for the trigger and for off-line analysis. The system consisted of an argon flash lamp driven by a mercury pulser with fiber optics to pipe the light to each counter. A separate flash lamp served the lead and iron part of the calorimeter although both lamps were powered by a common driver. To monitor the gain of the flash lamp one fiber cable was directed to the face of a monitor phototube. Glued to the face of the monitor tube was a 0.01 μC Bi^{207} β source imbedded in the disk of plastic scintillator to provide a light pulse of constant amplitude for comparison with the light flasher. A sketch of the system is shown in Fig. 7.

The photo tubes were selected and used gain stable bases.[3] Gain stability for the monitor over the full range of anode current was better than 2%. It was found that the tubes of the calorimeter had sufficiently good long-term stability that the average of a number of the most stable could be also used to monitor the level of the light flasher output.

In operation the flasher system was triggered several times each accelerator cycle within a special gate between spills.

IV. THE CALORIMETER READOUT SYSTEM

Signals were taken from the anode and the last dynode in each of the phototubes. The dynode signals were used in the trigger logic while the anode signals (transformer inverted at the base) were routed to CAMAC ADC's. Since the trigger was derived from a threshold on the transverse momentum, it was necessary to construct a signal

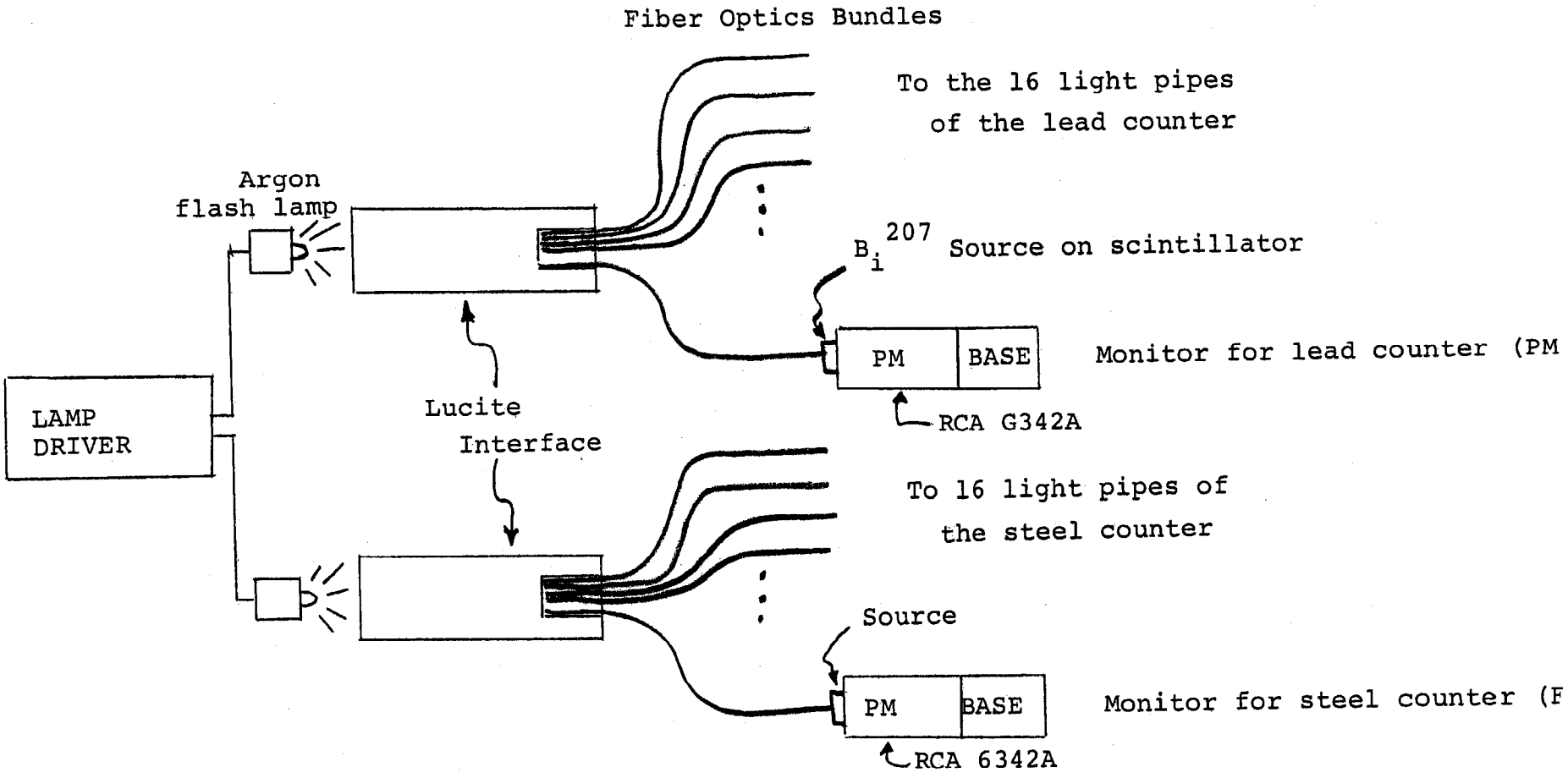

Figure 7

PHOTOTUBE GAIN MONITOR SYSTEM

proportional to P_t. The transverse momentum of a jet of particles may be characterized as follows:

$$P_t = (P_x^2 + P_y^2)^{1/2}$$

where P_x and P_y are the x and y components of the momentum of the jet (refer to Fig. 2).

$$P_x \tilde{=} \sum_i P_i \frac{X_i}{L} , \quad P_y \tilde{=} \sum_j P_j \frac{Y_j}{L}$$

where the sums are taken over the x and y counters and L is the distance from the target to the calorimeter. If f_{xi} is the fraction of the total energy E_T which is deposited in the x counter i P_t may be written:

$$P_t^2 = \frac{1}{L^2} \left(\sum_i f_{xi} E_T X_i\right)^2 + \frac{1}{L^2} \left(\sum_j f_{yj} E_T Y_j\right)^2 .$$

A signal approximately proportional to the transverse momentum was formed by adjusting the gains of the phototubes on both the x (horizontal) and y (vertical) strips so that they were weighted according to their mean polar angle from the target. The weighted pulse heights were then summed.

$$P_t \tilde{=} \Sigma \left(P_{xi} W_{xi} + P_{uj} W_{uj}\right)$$

where $P_{xi} W_{xi}$ and $P_{ui} W_{ui}$ are the weighted pulse heights for the horizontal and vertical counters. A trigger threshold set on this signal gives a reasonably sharp cut off on P_t.

V. CALIBRATION

Careful calibration was essential to the successful operation of

the calorimeter. The calibration proceeded in several steps. First, the gains of the lead and iron counters were determined using minimum ionizing particles (muons). The absolute calibration was measured by directing hadron and electron beams into all parts of the calorimeter. Finally the monitoring system was set up using the light flashers to continuously monitor the calibration during data taking.

Although initial calibration was carried out by moving the calorimeter around in the beam, subsequent calibration used a ten foot long pitching magnet of 38 kG-m located 45 feet upstream of the calorimeter. The pitching magnet was mounted on gimbles so that it could be rotated $\pm$ 40° about its longitudinal axis. The pitching magnet together with horizontal motion of the calorimeter (transverse to the beam) made it possible to direct a 20 GeV beam into all parts of the calorimeter.

The initial muon calibration was necessary to measure the relative gains of all the counters. Hadrons or electrons could not be used to balance x and y strips since the strips were separated by interaction material. In this stacking arrangement, x and y counters sample different parts of the longitudinal shower deposition producing a pulse height asymmetry. A muon trigger was set up using a scintillator telescope before and after the calorimeter and including a one-foot block of steel in front of the calorimeter. Because of the low light level for minimum ionizing particles, it was necessary to amplify the phototube signals typically by a factor of 4 before being fed to the ADC's. Both the muon peak and the light flasher peak were recorded for each of the counters. The phototube high voltages could then be adjusted using the light flashers to give relative weights to

the counters according to their polar angle from the target.

The absolute energy calibration was made by means of particle beams of 10, 20, 30 and 40 GeV/c momenta. Electrons were tagged 60 GeV by beam Cerenkov counters. Since pulse heights from the lead and steel counters were summed to give the trigger signal, it was necessary to balance the relative gain of the two parts. The gains were set so that the detector had the same response to beams of electrons and hadrons of the same energy. The validity of this gain assignment was checked by observing the behavior of the resolution of the total counter as a function of the relative gain of the two parts. For electrons incident only 20% of the energy is measured by the steel calorimeter and resolution is insensitive to the relative gain of the two parts of the counters. Hadron initiated showers fluctuate much more than those from electrons and often deposit a substantial fraction of their energy in the load. Typically 30% of the hadrons deposit more than 10% of their energy in the load. When the gains of lead and steel counters are set to give the same response for electrons and hadrons, the resolution for hadrons is at the bottom of a broad minimum.

During data taking, the calibration was monitored by means of the light flasher system. The gains of most of the 32 tubes remained constant within about $\pm$ 5%. A few of the tubes, however, showed varying degrees of gain drift outside this limit. The high voltages of these tubes were adjusted periodically throughout the runs to maintain a reliable trigger threshold.

Once or twice during each data taking run (about eight week duraction), low energy beams were swept across the calorimeter with the pitching magnet to check both the energy calibration and the relative gains of the counters. The level of the light flasher signal relative

to the shower signal would sometimes vary from run to run. This effect may have been due to a degradation of the light coupling of the fiber optics cable to the phototube or the gradual deterioration of the scintillator over the two-year span of the experiment.

VI. PERFORMANCE

The response to a well collimated beam of 20 GeV/c particles incident on the calorimeter, is shown in Figs. 8 through 10. Figure 8 shows the energy response for 20 GeV/c hadrons and electrons incident. Together with the energy response curve for the total calorimeter are curves showing the contributions of the lead and steel parts to the total energy. As electrons and hadrons are separated by a Cerenkov counter with threshold set for electrons, a muon peak appears on the hadron plot with a factor of 10 lower pulse height than the hadron peak. These measurements were made with the beam directed at the center of one of the counters. On the average, the resolution for electrons is somewhat worse because the showers sometimes straddle the crack between adjacent scintillator strips. Since the cracks are up to 1 mm wide and the core of a typical high energy electron shower is about 15 mm, significant energy can be lost in the cracks. In the case of hadron cascades, the core is typically 100 mm wide and cracks do not produce a noticeable effect. The resolution is sufficiently good, however, for electromagnetic showers (compared to hadronic showers) that the cracks do not limit the overall resolution of the calorimeter.

The contribution to the total calorimeter energy from the lead and steel parts are shown in Fig. 8. Figures 9 and 10 show the contributions of the x (horizontal) and y (vertical) strips to the total lead and steel energies for beams of electrons and hadrons respectively.

For most hadron events the entire energy is deposited in the steel. The hadron energy deposition in the lead however has a long

FIGURE 8

CALORIMETER ENERGY RESPONSE

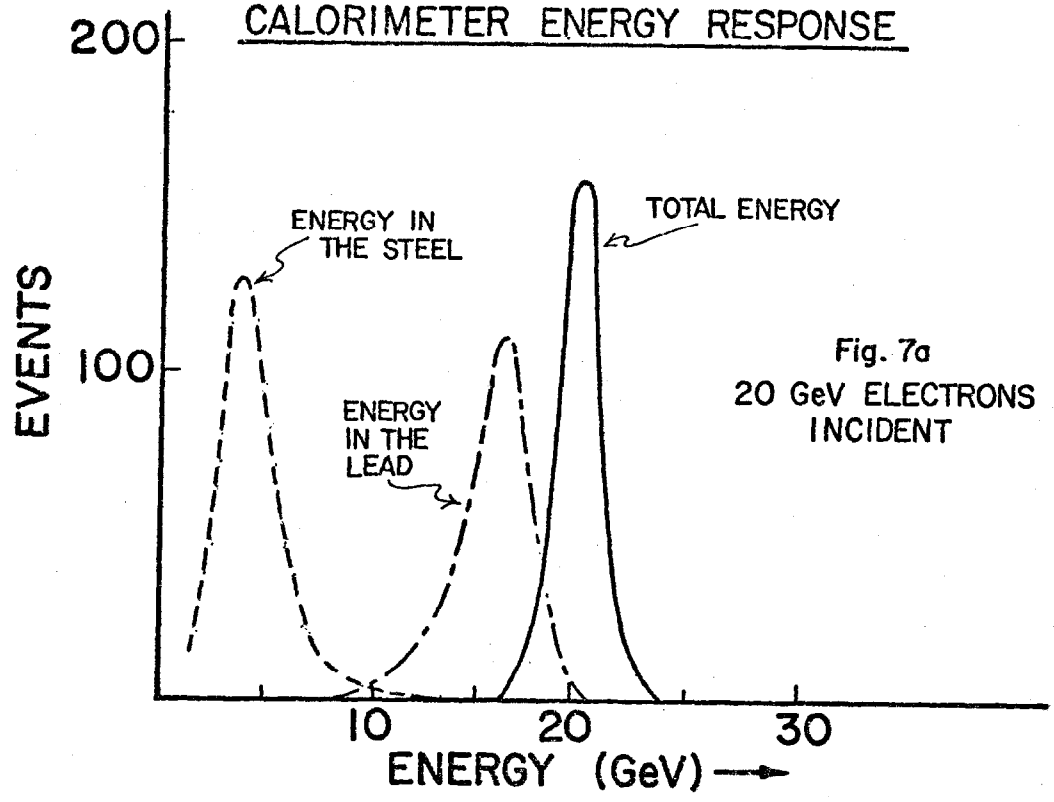

Fig. 7a
20 GeV ELECTRONS INCIDENT

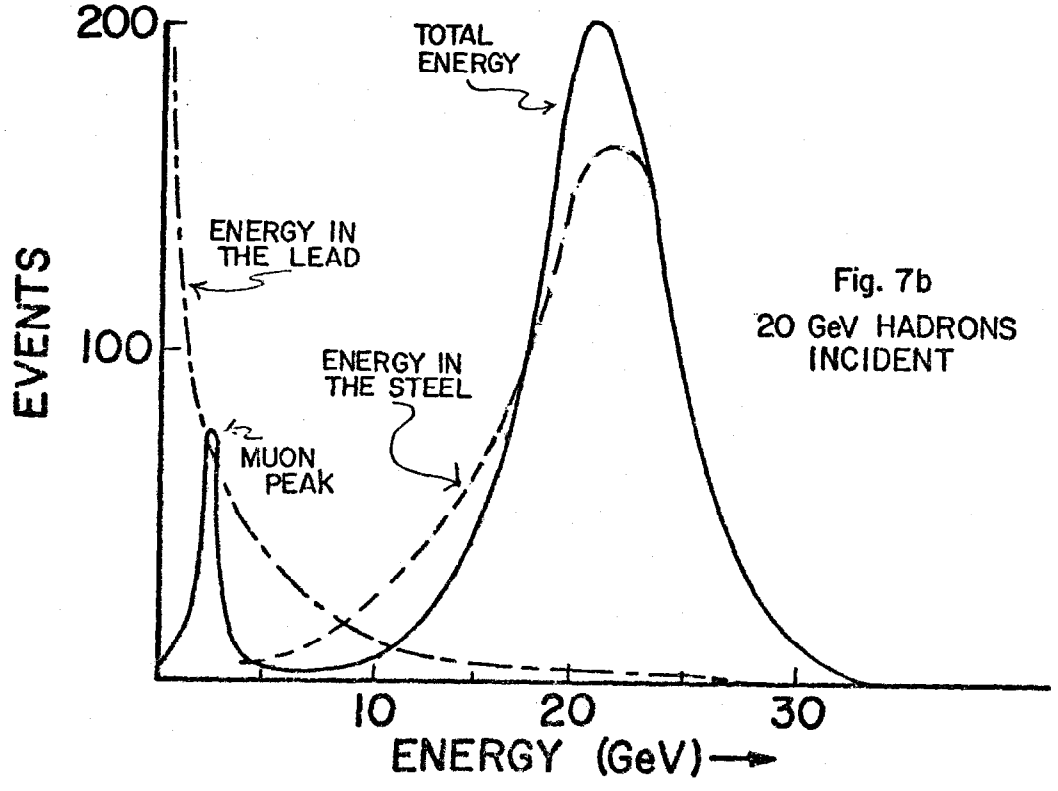

Fig. 7b
20 GeV HADRONS INCIDENT

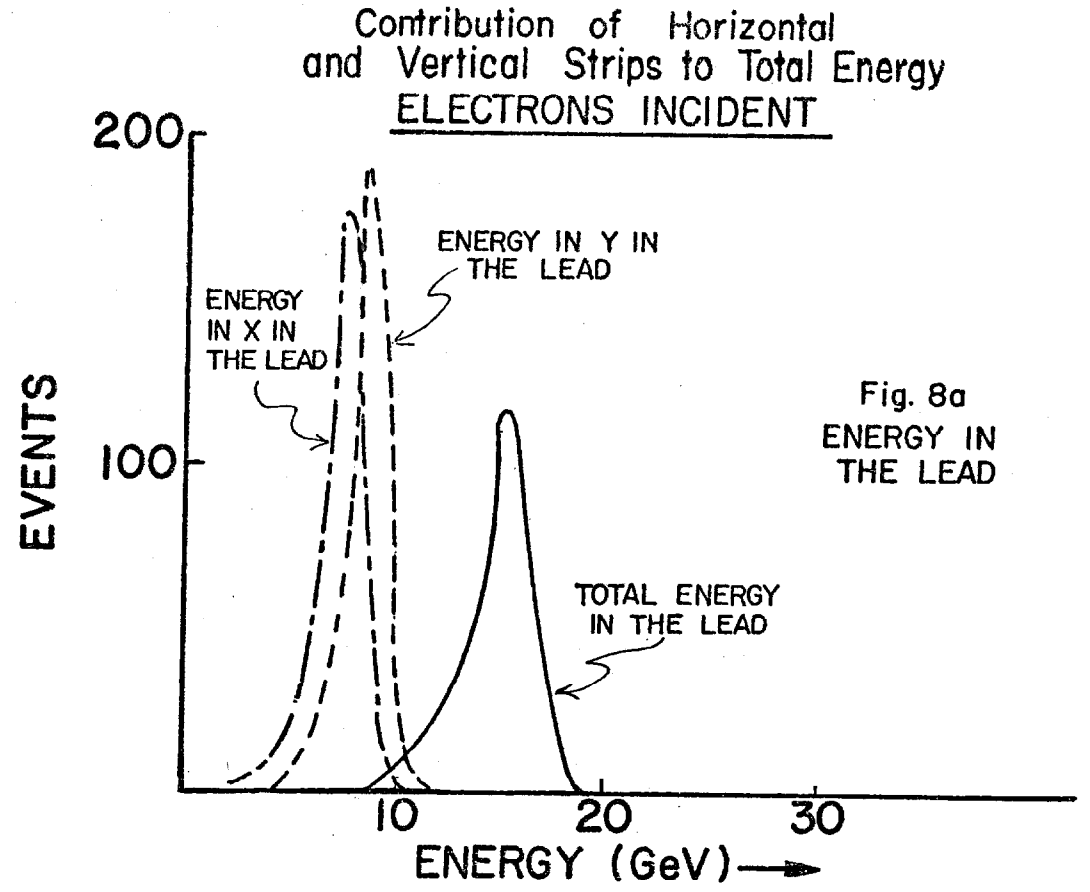

Fig. 8a
ENERGY IN
THE LEAD

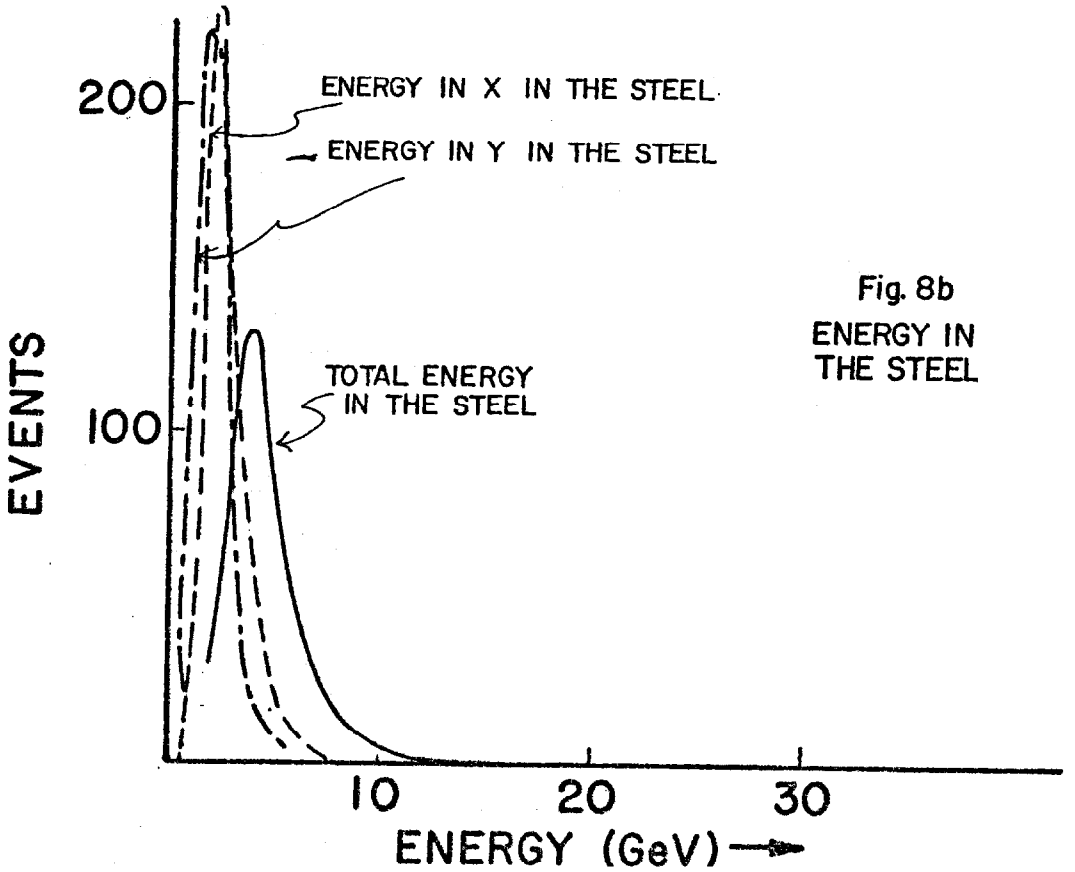

Fig. 8b
ENERGY IN
THE STEEL

Contribution of Horizontal and Vertical Strips to Total Energy

HADRONS INCIDENT

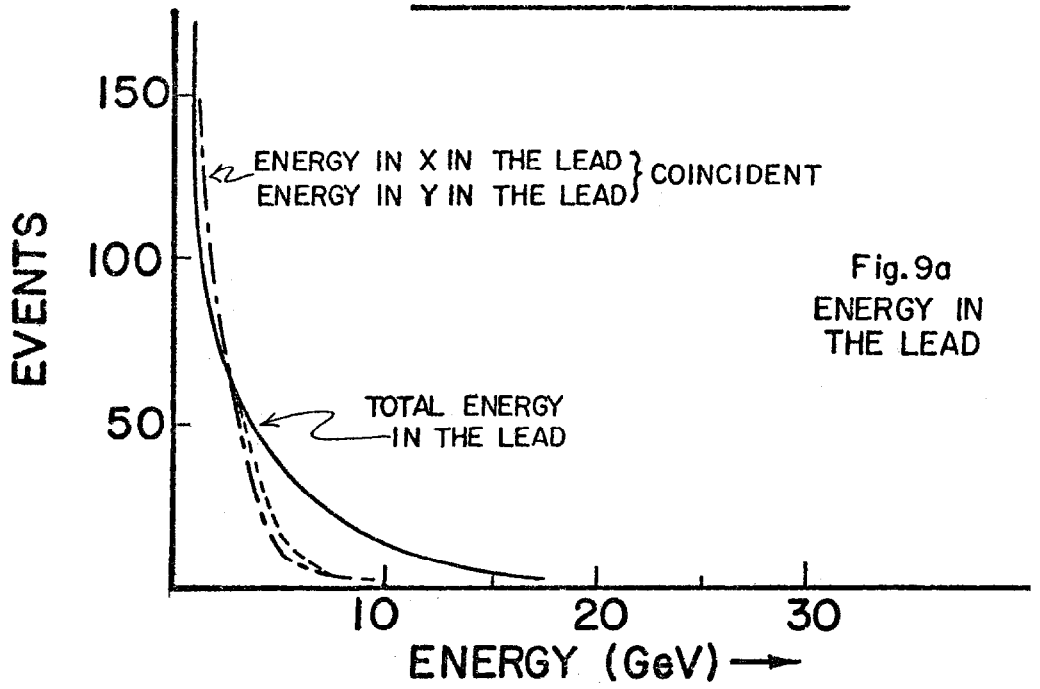

Fig. 9a
ENERGY IN THE LEAD

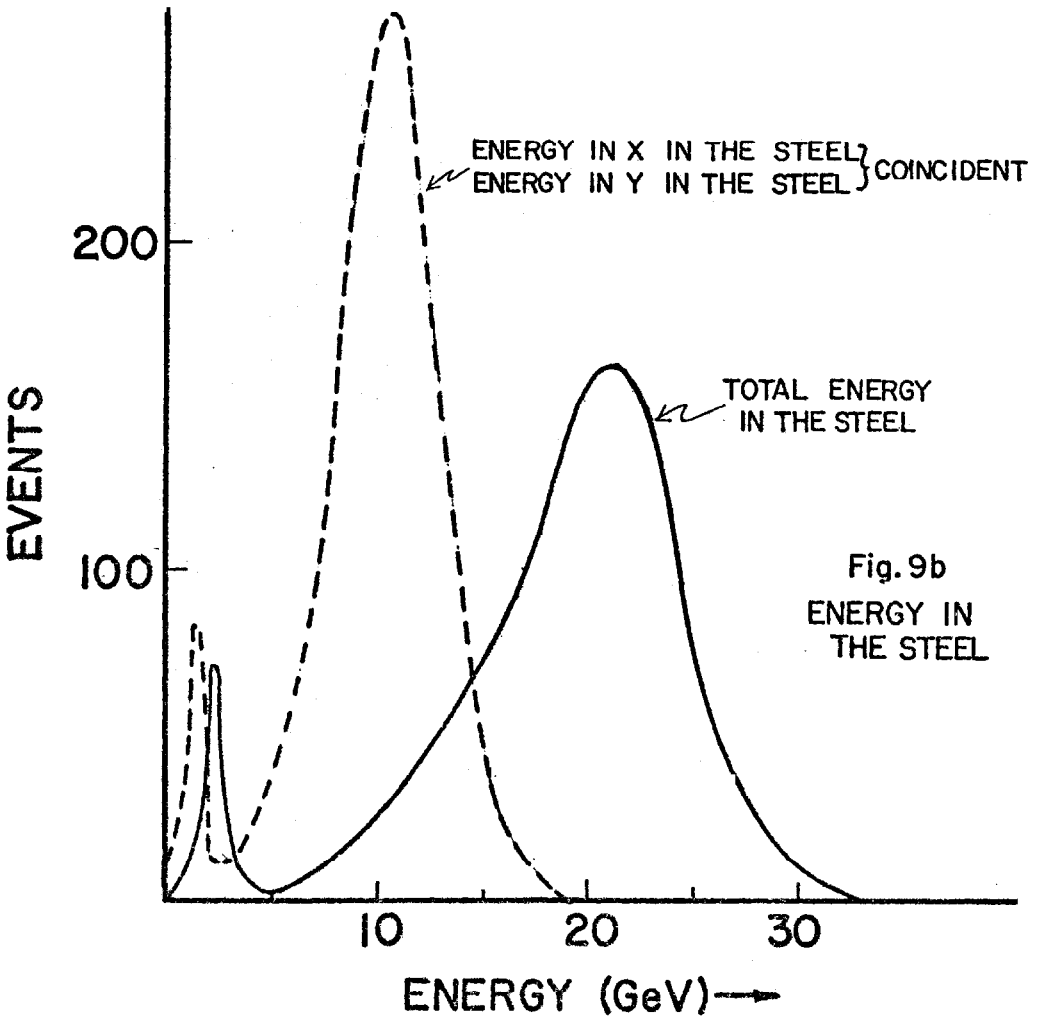

Fig. 9b
ENERGY IN THE STEEL

tail going out to nearly the total energy of the beam. Comparing the energy deposited in the lead and that in the steel with the total deposited energy shows how adding the lead energy removes the low energy tail on the total peak and sharpens the resolution. Since the lead counter has only 10 radiation lengths, a significant fraction of the energy from electron-initiated events (about 17% on the average) ends up in the steel.

The resolution from the curves in Fig. 8 is 12% FWHM (σ = 0.05) for electrons and 35% FWHM (σ = 0.15) for hadrons. The resolution for the x and y contributions separately in the lead for electrons and in the steel for hadrons is about $\sqrt{2}$ larger than the total energy resolution as expected for statistically independent sampling. Since the number of photons per minimum ionizing particle (muons) is about 25, and 20 GeV hadrons produce ten times the light, there is a negligible contribution from photon statistics.

Another feature of the response curves is the asymmetry between x and y counter strips with electrons incident. The asymmetries arise because x and y counters sample different parts of the shower. A calculation of the expected x,y asymmetry in the lead using measured electron longitudinal energy deposition curves, shows rough agreement with the data. Little x and y asymmetry is expected in the case of incident hadrons as the energy deposition by hadrons is much flatter. Figure 11 shows the asymmetries in the lead and steel for hadrons and electrons. For the electrons in the lead the y counter strips sample on the average more energy than the x counters. When the electron showers enter the steel they penetrate only a few counters and since the x strips are first encountered somewhat more energy is sampled there.

The response of the calorimeter and the associated resolution were measured for electron and hadron beams of 10, 20, 30 and 40 GeV/c momentum. The response for electrons (Fig. 12) and hadrons (Fig. 13)

FIGURE 11
ASYMMETRY IN ENERGY

$$R = \frac{E_x - E_y}{E_x + E_y}$$

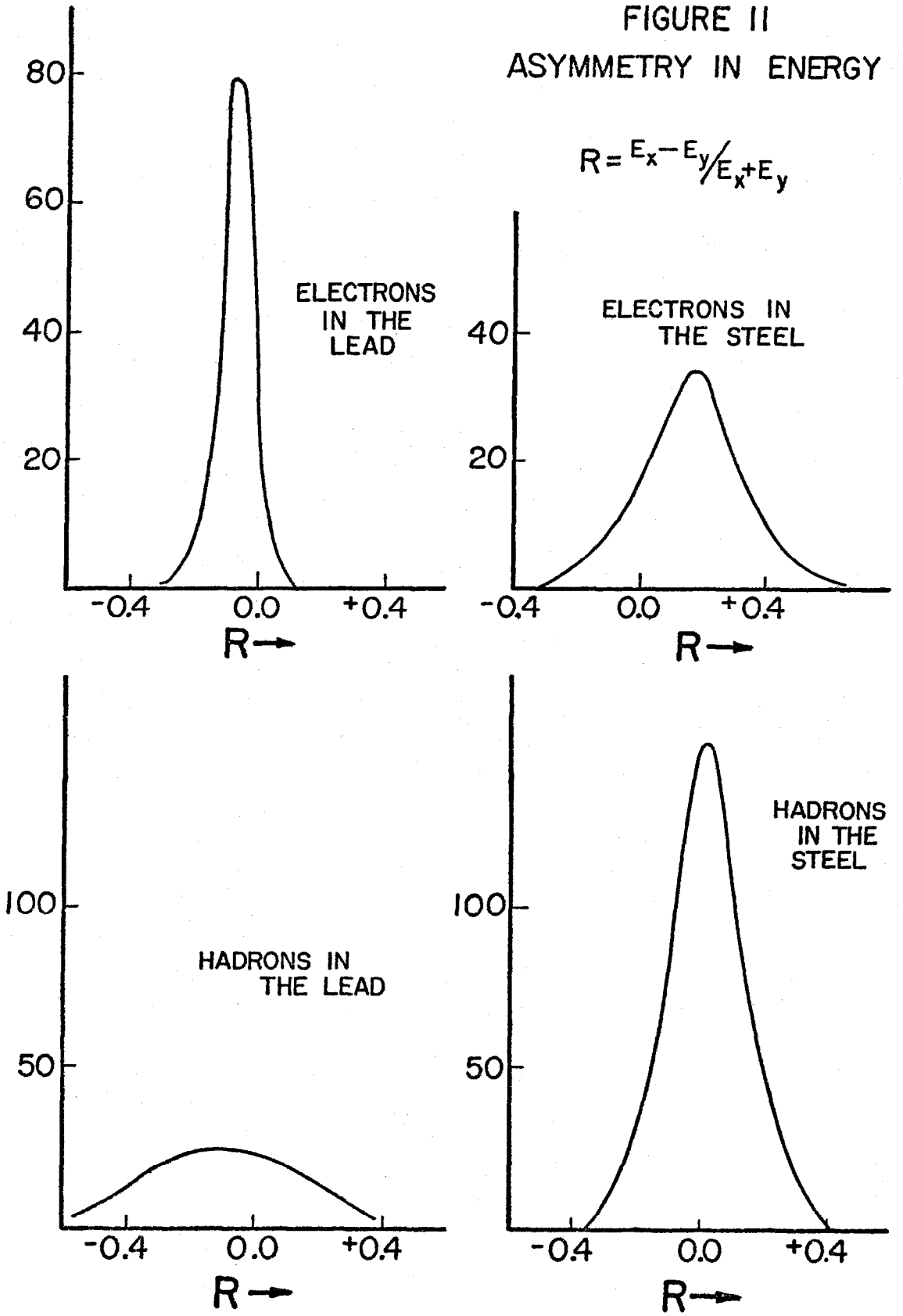

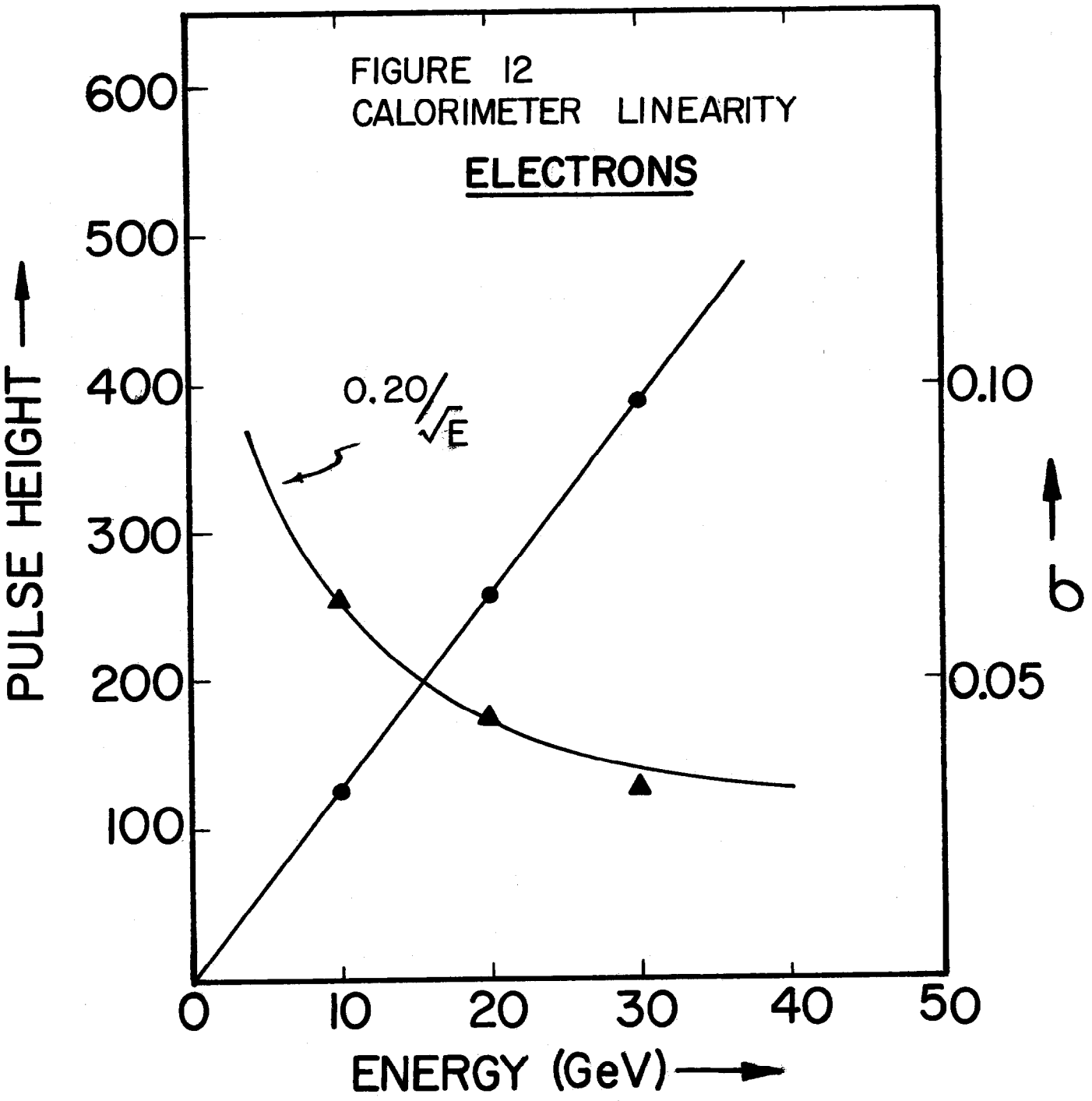
FIGURE 12
CALORIMETER LINEARITY
ELECTRONS
0.20/√E
PULSE HEIGHT
600
500
400
300
200
100
0.10
0.05
b
0
10
20
30
40
50
ENERGY (GeV)

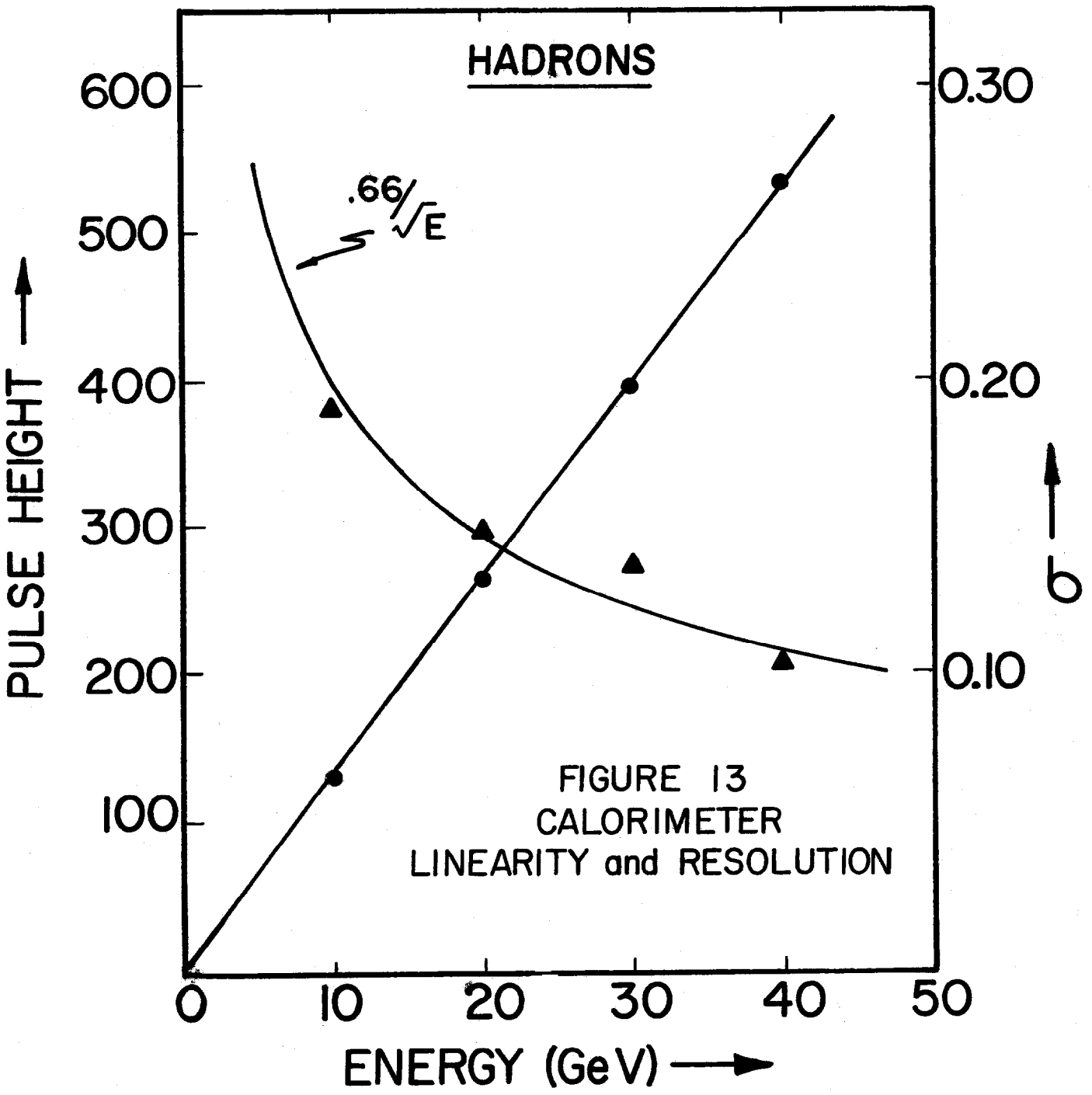

FIGURE 13
CALORIMETER
LINEARITY and RESOLUTION

is linear to within ± 1% over the range measured. (Early in the testing of the calorimeter fully in the beam, the response was found to be linear within ± 3% up to 120 GeV.) The resolution variation with energy for electrons and hadrons is also shown. The resolution functions assuming a $1/\sqrt{E}$ dependence are best described as follows:

$$\frac{\Delta E}{E}\ (\text{FWHM}) = 0.46/\sqrt{E}$$

Electrons

$$(\sigma = 0.20/\sqrt{E}).$$

$$\frac{\Delta \varepsilon}{\varepsilon}\ (\text{FWHM}) = 1.6/\sqrt{E}$$

Hadrons

$$(\sigma = 0.66/\sqrt{E})$$

The overall depth of the calorimeter was 5.3 absorption length. It is reasonable to examine the calibration data for evidence of energy leakage out the back. Even at 40 GeV there is no apparent degradation of calorimeter response. The resolution curve, Fig. 13, is also still falling smoothly at the highest energy.

It should be noted that the resolution of hadron calorimeters of the type described here is expressed in parameters of the normal distribution. The distribution however has tails which depart significantly from Gaussian. For a calorimeter measurement of the p_T variation of the cross section the shape of the tails, particularly the high energy tail, is critical. Since the cross section falls so rapidly ($\sim e^{-2.3p_T}$) the high energy tail has the effect of smearing events to higher transverse momentum. The data therefore must be carefully corrected for this smearing. Figure 14 shows a log plot of the energy response to a large sample of hadrons at

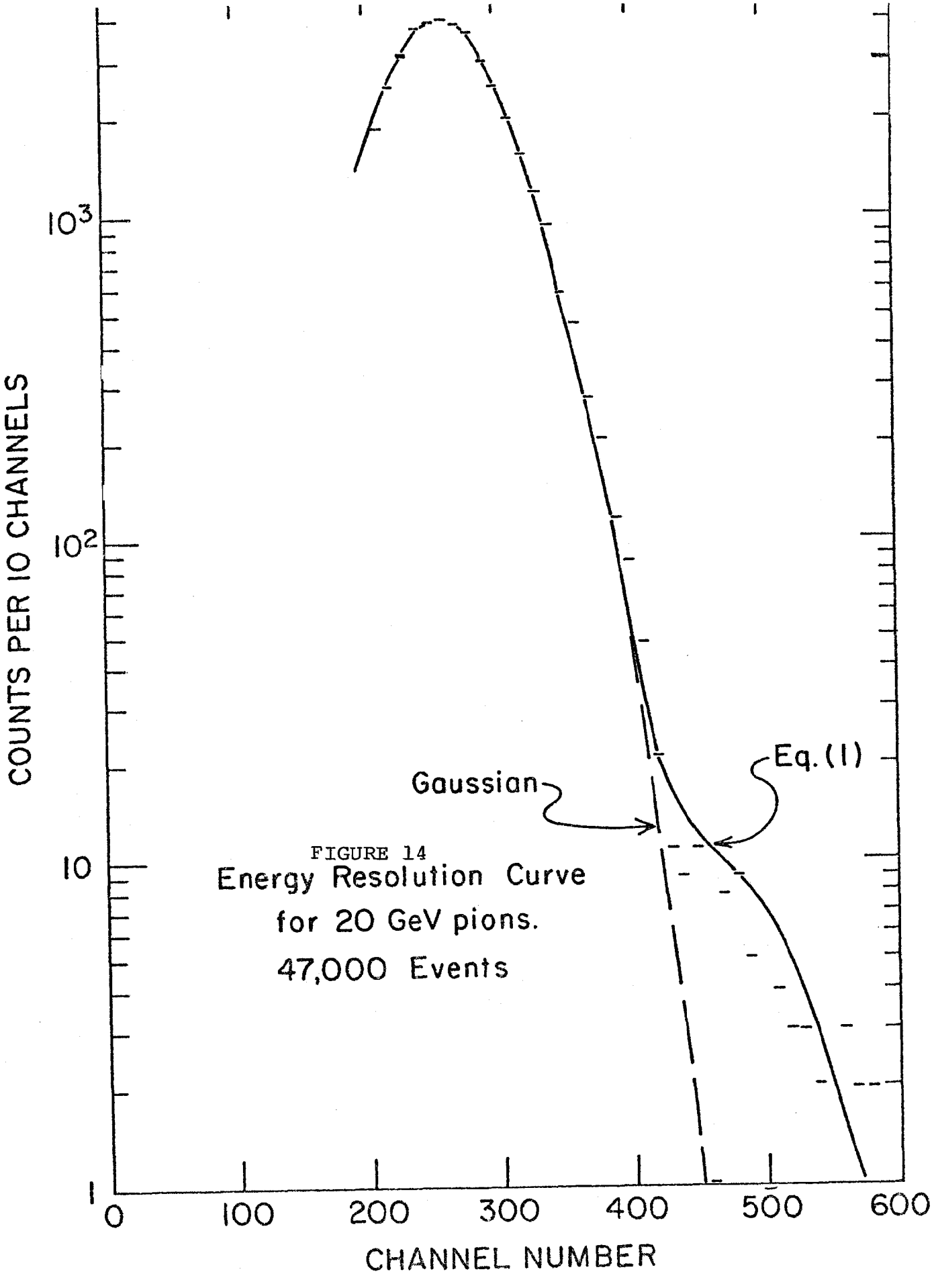

FIGURE 14
Energy Resolution Curve
for 20 GeV pions.
47,000 Events

20 GeV. The response falls in a gausian shape but also has a shoulder at large pulse height. The following sum of two gausians gives a reasonable functional fit to the curve:

$$F(E,E_0) = 0.997\ G_1(E,E_0) + 0.003\ G_2(E,1.7E_0)$$

where

$$G(E,E_0) = \frac{1}{\sigma(E_0)} \frac{1}{\sqrt{2\pi}} \exp[-(E-E_0)^2/2\sigma^2],$$

$$\sigma_1 = 0.81\sqrt{E_0} \qquad \sigma_2 = 1.0\sqrt{E_0} \quad .$$

The events in the tail undoubtedly occur when a pion making a first collision in the iron, gives essentially all of its energy to π^0's. Electromagnetic showers are converted to scintillation light more effectively in iron by a factor of about 1.5 due to nuclear disintegration and poor scintillator response to high ionization density. It has been calculated that a 20 GeV pion gives more than 90% of its energy to π^0's 0.2-0.3% of the time. The location and width of the tail are consistent with this hypothesis.

Since a jet is a cluster of particles rather than a single particle as used in the calibration it is important to demonstrate that the resolution for single particles and jet is the same. This effect can be studied by requiring that the hadron interact in the lead thereby producing several particles that enter the steel calorimeter. This can be done by selecting events with more than twice but less than five times minimum ionizing in the lead. The result is shown in Fig. 15 where the resolution for the selected events is compared with the total sample. The resolution for this special sample is slightly better because of the better resolution for the electromagnetic component in the lead.

As previously mentioned the calibration was accomplished by sweeping a 20 GeV/c momentum beam over the face of the calorimeter. The data (hadrons, electrons and muons) were used to adjust the gains of the individual strips to yield a uniform response over the whole calorimeter. The result was a uniformity with $\pm$ 2% of the incident energy and $\pm$ 5% in resolution to within 10 cm of the edges. Figure 16 shows the response and resolution for a typical sweeps across the calorimeter including edge effects. The circle indicates the size of the incident beam. The diffuse edge results from the calibration beam being at a slightly smaller angle than the edge of the calorimeter. The sweep demonstrates that the response is smooth and uniform across the calorimeter. The response for electrons is full at about 3 cm inside the calorimeter while for hadrons the particle must hit about 10 cm inside the edge of the calorimeter before full energy capture is approached. The "size" of the hadronic shower integrated longitudinally can be examined by plotting the distribution of energy in the x counterstrips in the steel for a localized beam of hadrons. The result is shown in Fig. 17. This distribution can be used to estimate that 85% of the energy in the shower will be contained in the calorimeter if the particle hits five cm from the edge. This is consistent with the behavior of the response at the calorimeter edge as shown in Fig. 16.

Since the transverse momentum consists of the product of angle and energy shower position determination is important. Because of the spreading of the energy among several adjacent counters, the weighted position of the center of the shower is more accurately known than one counter width. With a pencil beam incident on the

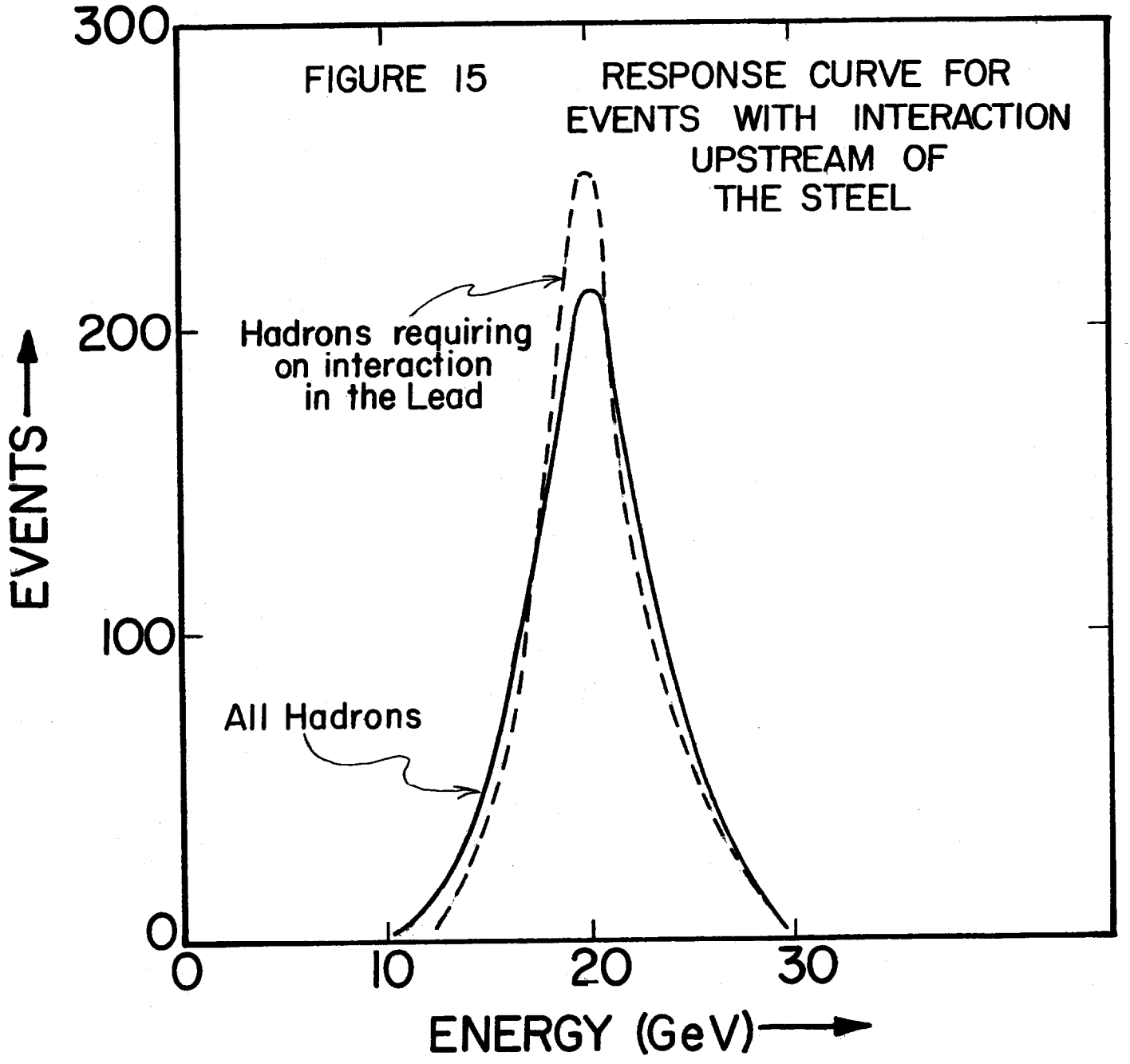

FIGURE 15 RESPONSE CURVE FOR EVENTS WITH INTERACTION UPSTREAM OF THE STEEL

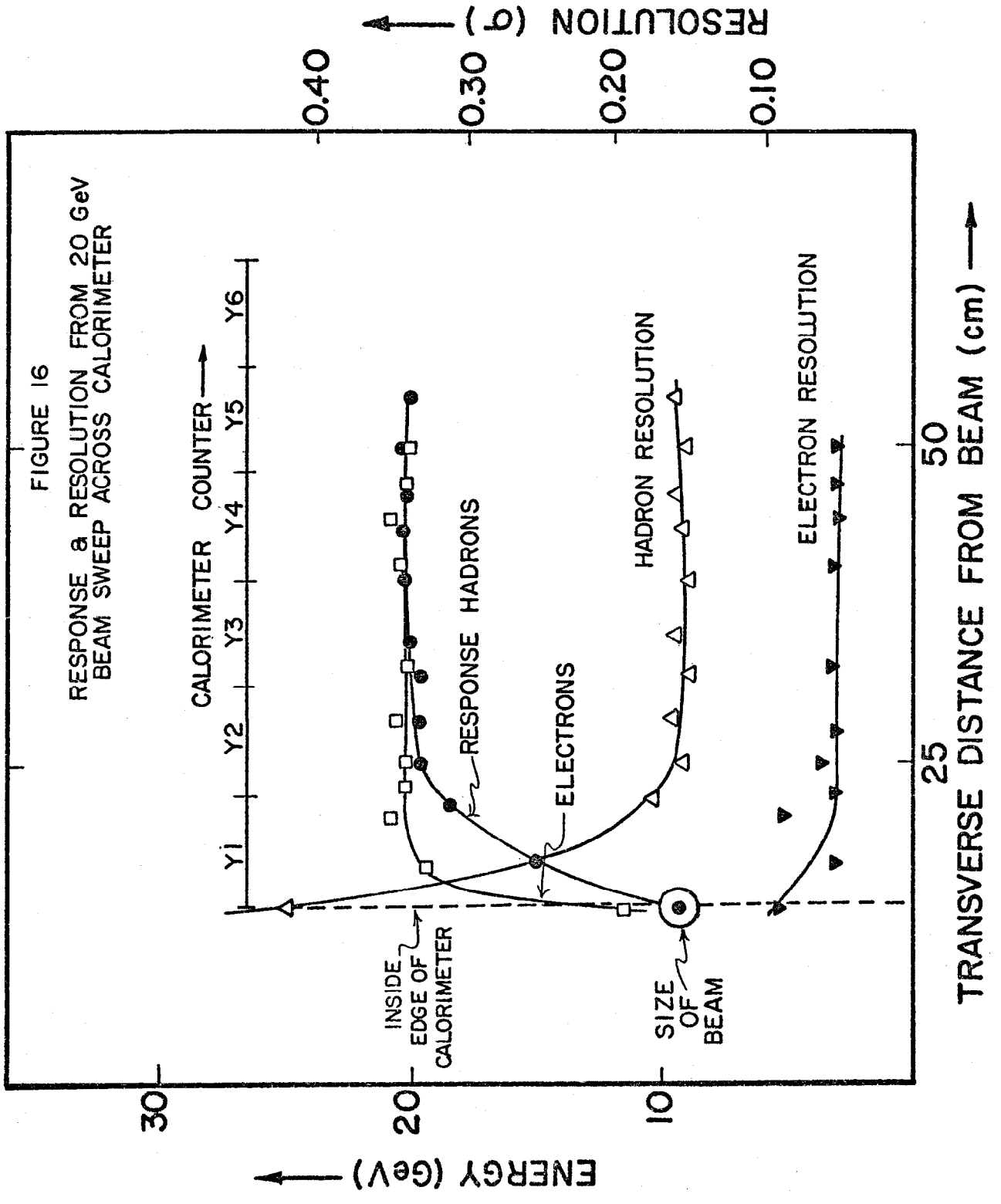
FIGURE 16
RESPONSE & RESOLUTION FROM 20 GeV
BEAM SWEEP ACROSS CALORIMETER
CALORIMETER COUNTER
Y1
Y2
Y3
Y4
Y5
Y6
RESPONSE HADRONS
ELECTRONS
HADRON RESOLUTION
ELECTRON RESOLUTION
INSIDE EDGE OF CALORIMETER
SIZE OF BEAM
ENERGY (GeV)
30
20
10
RESOLUTION (σ)
0.40
0.30
0.20
0.10
25
50
TRANSVERSE DISTANCE FROM BEAM (cm)

on the calorimeter (away from the edge) the center of energy distribution for the x counters was plotted for a number of events. The beam was limited to be $\pm$ 1.3 cm. At half maximum the width is $\pm$ 1.5 cm as shown in Fig. 18 (each x-counter is 10 cm wide).

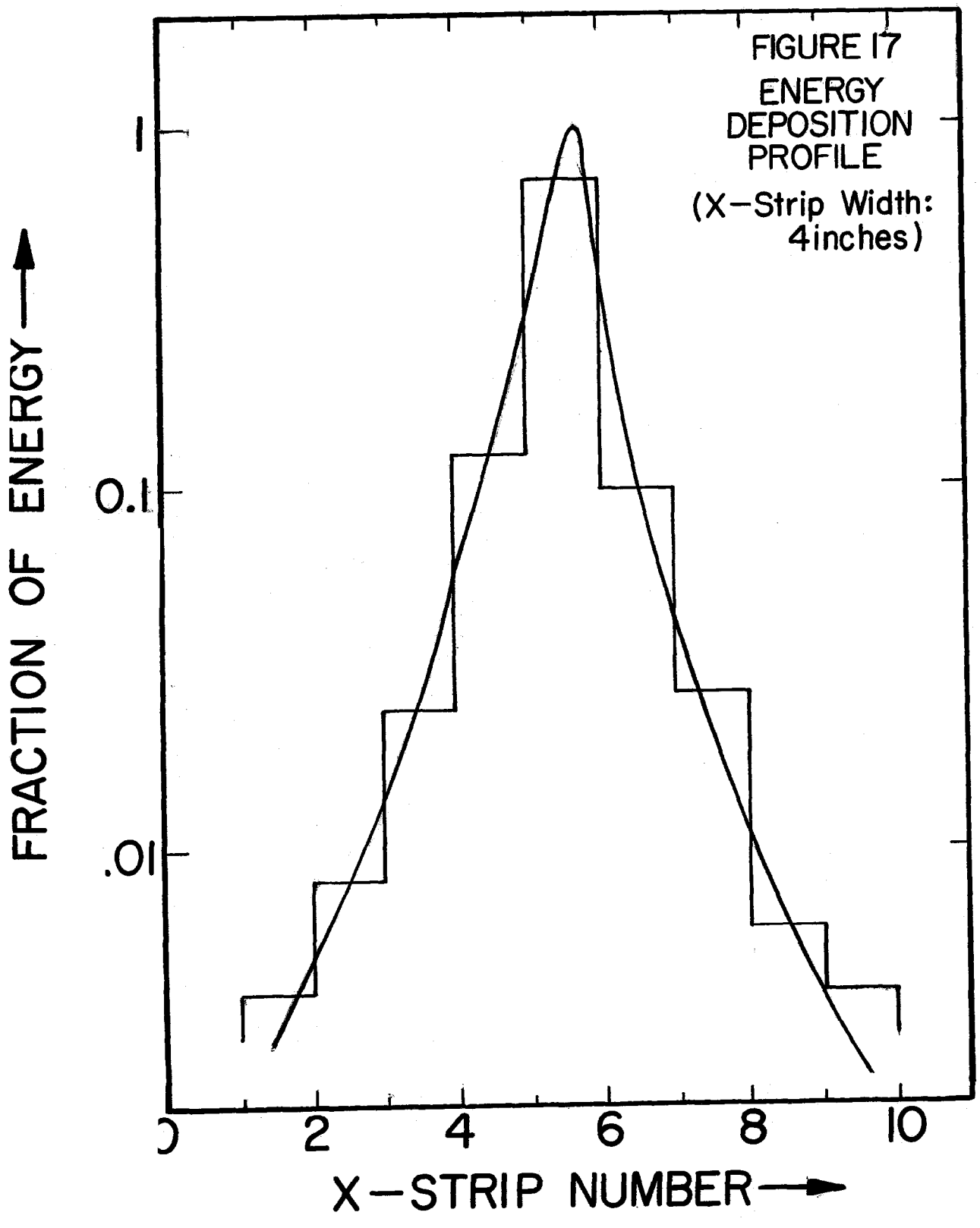
FIGURE 17
ENERGY DEPOSITION PROFILE
(X-Strip Width: 4inches)
FRACTION OF ENERGY
1
0.1
.01
0
2
4
6
8
10
X-STRIP NUMBER

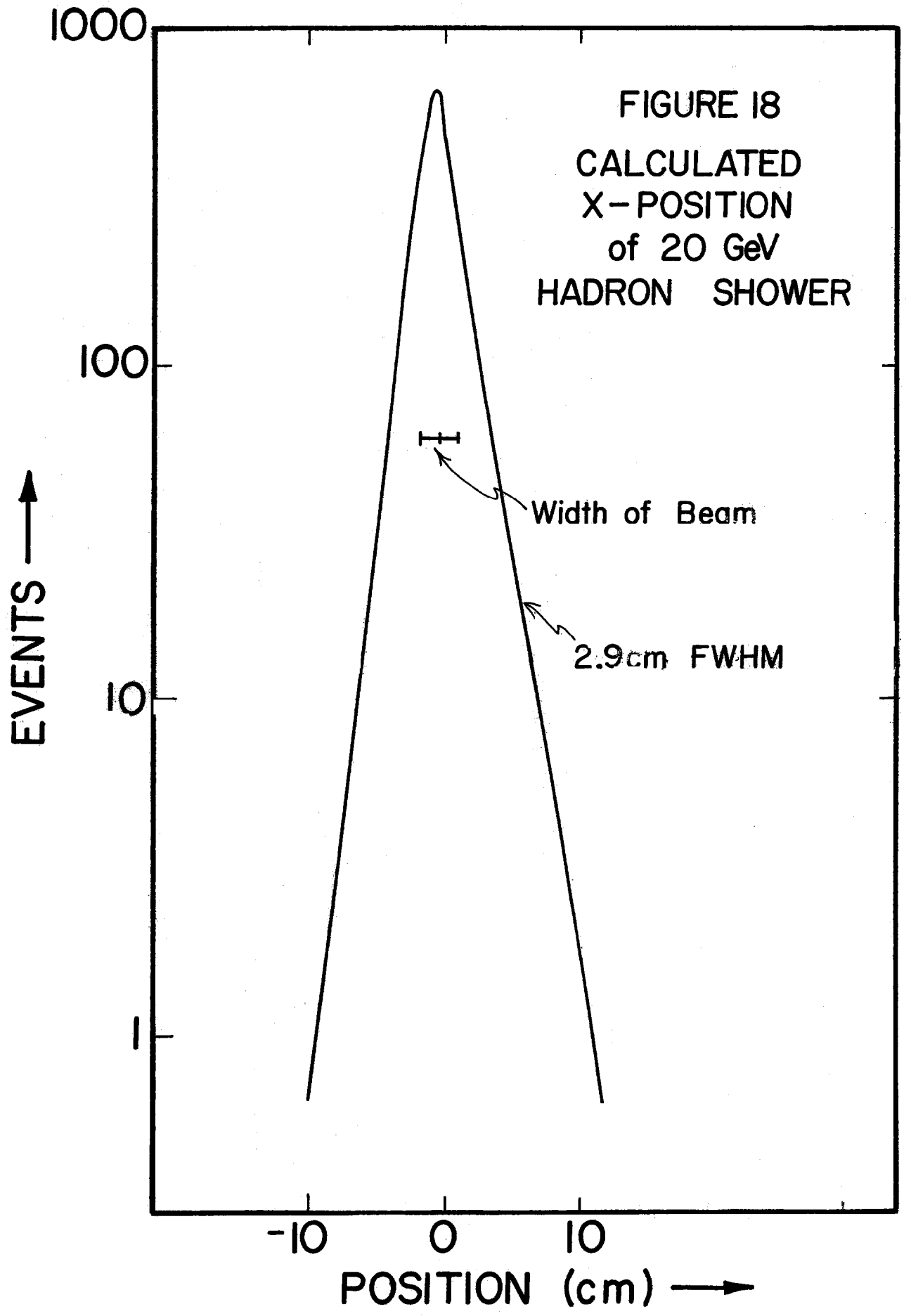
1000
100
10
1
EVENTS
FIGURE 18
CALCULATED
X-POSITION
of 20 GeV
HADRON SHOWER
Width of Beam
2.9cm FWHM
-10
0
10
POSITION (cm)

References

1. Walker, R., Caltech, private communication.
2. Kerns, C.R., Gain Stability Measurements Techniques for Calorimeter Phototubes, Proceedings of the Calorimeter Workshop, M. Atac, Editor, Fermi National Accelerator Laboratory, Batavia, Illinois, May 1975.
3. Kerns, C.R., A High-Rate Phototube Base, Fermilab Technical Memo 640, January 22, 1976.